Virologica Sinica 41 (2026) 676–687

Contents lists available at ScienceDirect

Virologica Sinica

journal homepage: www.keaipublishing.com/en/journals/virologica-sinica
www.virosin.org

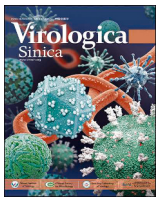

Research Article

Therapeutic efficacy of a K1-specific bacteriophage against hypervirulent *Klebsiella pneumoniae* in a mouse infection model

Xiaona Yan [a,b], Mengmeng Su [a,b], Sixiang Xu [a,b], Xiangkuan Zheng [a,b], Xiaoyue Li [a,b], Peifan Liu [a,b], Yilin Fang [a,b], Libin Tan [a,b], Long Chen [c], Hong Du [d], Panpan Tong [e], Yuxia Zhang [f], Qinghai Ren [g,*], Wei Zhang [a,b,*]

[a] MOE Joint International Research Laboratory of Animal Health and Food Safety, College of Veterinary Medicine, Nanjing Agricultural University, Key Lab of Animal Bacteriology, Ministry of Agriculture, Nanjing 210095, China
[b] The Sanya Institute of Nanjing Agricultural University, Yabulun Industrial Park, Yazhou Bay Science and Technology City, Sanya 572024, China
[c] Department of Clinical Laboratory, Zhangjiagang Hospital Affiliated to Soochow University, Zhangjiagang 215600, China
[d] Department of Clinical Laboratory, The Second Affiliated Hospital of Soochow University, Suzhou 215004, China
[e] Tianshui Municipal Center for Disease Control and Prevention, Tianshui 741000, China
[f] College of Veterinary Medicine, Xinjiang Agricultural University, Wulumuqi 830052, China
[g] Phage Research Center, School of Agriculture and Biology, Liaocheng University, Liaocheng 252000, China

ARTICLE INFO

Keywords:
Klebsiella pneumoniae
Bacteriophage
Hypervirulent
K1
Mouse infection model

ABSTRACT

Klebsiella pneumoniae is an important opportunistic pathogen in both humans and animals. Controlling it has become increasingly difficult due to the rapid spread of antimicrobial resistance. In this study, we isolated and characterized a novel lytic bacteriophage, vB_Kp_Z1, and evaluated its therapeutic efficacy against K1-serotype *K. pneumoniae*. Host range analysis showed that vB_Kp_Z1 was strictly specific to K1 strains, as confirmed across multiple prevalent capsular types. The *in vivo* efficacy of vB_Kp_Z1 was assessed using intraperitoneal infection models in mice. Two hypervirulent K1 strains were used: a pigeon-derived strain (KP1897) and a human clinical strain (KP177). Phage treatment significantly improved survival compared with phosphate-buffered saline-treated controls. It provided complete protection in KP1897-infected mice and achieved an 87.5% survival rate in KP177-infected mice. In addition, phage administration markedly reduced bacterial loads in the blood, liver, and lungs, indicating effective control of systemic dissemination. These findings demonstrate that vB_Kp_Z1 is a K1-specific bacteriophage with therapeutic potential against hypervirulent *K. pneumoniae*, including strains from different host species.

INTRODUCTION

Klebsiella pneumoniae is a Gram-negative, facultative anaerobic opportunistic pathogen. It colonizes the respiratory, gastrointestinal, and genitourinary tracts of humans and animals. It is a major cause of pneumonia, urinary tract infections, bloodstream infections, and pyogenic liver abscess worldwide (Lin et al., 2024). *K. pneumoniae* strains are commonly divided into classical (cKP) and hypervirulent (hvKP) lineages based on virulence characteristics. The classical lineage (cKP) primarily causes hospital-acquired infections and typically affects immunocompromised individuals. In contrast, the hypervirulent lineage (hvKP) is associated with community-acquired infections and can cause severe invasive disease even in immunocompetent hosts (Russo and Marr, 2019; Liao et al., 2024). A defining feature of hvKP is the hypermucoviscous phenotype, identified by a positive string test and associated with the overproduction of capsular polysaccharides (Hsu et al., 2011). Among the numerous capsular serotypes, K1 is one of the most prevalent types associated with hvKP. It is strongly associated with liver abscess formation, resistance to neutrophil-mediated killing, and escape from serum bactericidal activity (Wang et al., 2017; Choby et al., 2020;

* Corresponding authors.
E-mail addresses: vszw@njau.edu.cn (W. Zhang), renqinghai113@126.com (Q. Ren).
Peer review under the responsibility of editorial board of *Virologica Sinica*.

https://doi.org/10.1016/j.virs.2026.06.003
Received 18 January 2026; Accepted 1 June 2026
Available online 4 June 2026

Kim et al., 2020). The capsular layer facilitates immune evasion and promotes biofilm formation, contributing to bacterial persistence and reduced antibiotic efficacy (Mohammed and Zgair, 2025). *K. pneumoniae* forms biofilms on both biotic and abiotic surfaces through capsular polysaccharides and fimbrial adhesins. Biofilm-associated cells exhibit increased tolerance to antibiotics and host immune defenses, leading to persistent infection and reduced treatment efficacy (Vuotto et al., 2014; Sun et al., 2025).

The widespread use of broad-spectrum antibiotics has accelerated the emergence and dissemination of extended-spectrum β-lactamase- and carbapenemase-producing *K. pneumoniae*, resulting in increasingly limited treatment options (Agyeman et al., 2020; Fang et al., 2023). Concurrently, hvKP strains have been increasingly reported in animal reservoirs, including avian species such as pigeons, raising concerns about the circulation of hypervirulent and drug-resistant strains between animals and humans. These findings highlight the potential role of animal populations as reservoirs of hvKP and underscore the need for antimicrobial strategies effective against isolates from diverse host origins.

Bacteriophages are bacterial viruses that replicate intracellularly and typically exhibit high host specificity (Gradisteanu Pircalabioru et al., 2021; Ding et al., 2025). Interest in phage therapy has resurged in response to the global rise of antibiotic resistance, particularly for infections caused by multidrug-resistant *K. pneumoniae* (Mehta et al., 2025). Experimental studies have demonstrated that *K. pneumoniae* phages can inhibit planktonic bacterial growth, prevent biofilm formation, and disrupt established biofilms under *in vitro* (Senhaji-Kacha et al., 2024). Therapeutic efficacy has also been reported in animal models of pneumonia, bacteremia, liver abscess, and wound infection, where phage treatment significantly reduced bacterial burdens and improved survival rates (Zagaliotis et al., 2022). Some *K. pneumoniae* phages encode capsule depolymerases that degrade capsular polysaccharides, thereby facilitating access to the bacterial cell surface and enhancing phage-mediated killing of highly encapsulated hvKP strains (Jiao et al., 2025).

To evaluate the therapeutic breadth of the phage, this study isolated and characterized a novel K1-specific lytic phage, vB_Kp_Z1. Its therapeutic potential was then assessed in a murine systemic infection model using a representative pigeon-derived strain and a highly virulent human-derived K1 strain (KP177). The results showed that vB_Kp_Z1 effectively protected mice in infection models based on both strains. These findings highlight the potential of vB_Kp_Z1 as a therapeutic candidate for treating infections caused by hypervirulent K1 *K. pneumoniae* originating from different host origins.

RESULTS

K. pneumoniae virulence and resistance phenotypes

The human-derived strain KP177 showed a hypermucoviscous phenotype, confirmed by a positive string test (>5 mm) (Supplementary Fig. S1). MIC results showed resistance to three or more classes of antimicrobial agents (Supplementary Table S1). These phenotypic characteristics supported its selection for subsequent mouse infection experiments.

Morphological characteristics of the phage

Phage vB_Kp_Z1 formed distinct plaques on double-layer agar plates after 12 h of incubation with its host bacterium KP1897 at 37 °C. With prolonged incubation, a translucent halo appeared around the plaques and gradually expanded. suggesting the presence of a putative depolymerase (Fig. 1A). Electron microscopy showed that vB_Kp_Z1 belongs to the class *Caudoviricetes* (tailed phages). The phage exhibited an icosahedral head diameter of approximately 63 ± 1 nm and a tail length of about 15 ± 0.5 nm (Fig. 1B).

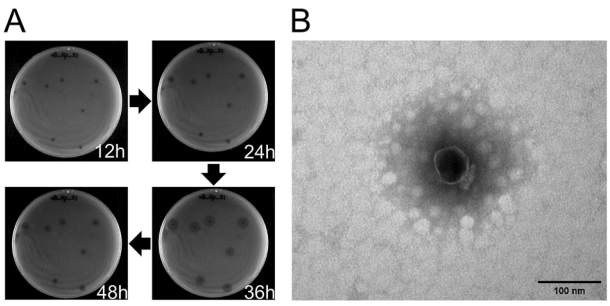

Fig. 1. Morphology of phage vB_Kp_Z1. **A** Plaque morphology of phage vB_Kp_Z1 observed at 12, 24, 36, and 48 h post-infection. **B** Transmission electron micrograph of phage vB_Kp_Z1 following negative staining with 2% (w/v) phosphotungstic acid. Scale bar, 100 nm.

Host range of phage vB_Kp_Z1 shows capsule-type specificity

The host range of phage vB_Kp_Z1 was evaluated using both spot assays and double-layer agar plaque assays. A total of 61 *K. pneumoniae* strains were tested, representing 26 distinct capsular serotypes. Lytic activity was observed exclusively against K1 serotype strains. No plaque formation or lysis zones were detected on strains belonging to other capsular types. Notably, vB_Kp_Z1 lysed all tested K1-type *K. pneumoniae* isolates (20/20), corresponding to a 100% lysis rate within this capsular serotype. In contrast, no lytic activity was observed against non-K1 *K. pneumoniae* strains or against other Enterobacteriaceae species tested in this study. The lysis patterns from spot assays were fully consistent with those from plaque assays. These results confirm that vB_Kp_Z1 exhibits a high degree of capsular type specificity for K1 *K. pneumoniae*.

Biological characterization of phage vB_Kp_Z1

To determine the optimal multiplicity of infection (MOI) for phage vB_Kp_Z1, co-culture experiments were performed using the host strain KP1897 at different MOIs. After 12 h of incubation, the highest phage titer was obtained at an MOI of 1, approximately 2.49×10^9 PFU/mL. This MOI was therefore selected as the optimal MOI. Phage amplification was detectable at an MOI of 10, but the final titer was lower than that obtained at the optimal MOI. In contrast, reduced phage yields were observed at MOIs of 0.1, 0.01, 0.001, and 0.0001 (Fig. 2A). One-step growth curve analysis showed a latent period of approximately 10 min, followed by a rapid rise phase. The phage titer peaked at 100 min and remained stable thereafter (Fig. 2B).

In the temperature and pH stability experiments, the phage vB_Kp_Z1 exhibited robust stability within the temperature range of 4 °C–37 °C and a pH range of 3–11. When the temperature increased to 50 °C and 60 °C, the survival rate significantly decreased to 59.1% and 2.69%, respectively. Complete loss of infectivity was observed at temperatures ≥70 °C (Fig. 2C). Notably, the phage maintained a high survival rate of 98% under strongly acidic (pH = 3) and strongly alkaline (pH = 10) conditions. However, no viable phages were detected under extreme pH conditions (pH = 2 and pH = 11) (Fig. 2D).

Genome annotation, comparative genomics, and phylogenetic analysis

The genome of bacteriophage vB_Kp_Z1 consists of linear double-stranded DNA, with a total length of 46,827 bp and a GC content of 45.62%. Whole-genome annotation analysis using Pharokka identified 61 CDSs, of which 34 CDSs encode proteins with known functions, while 27 CDSs encode hypothetical proteins of unknown function (Supplementary Table S2). Notably, tRNAscan-SE analysis revealed the presence of a serine tRNA gene (tRNA-Ser) in the genome, which may be

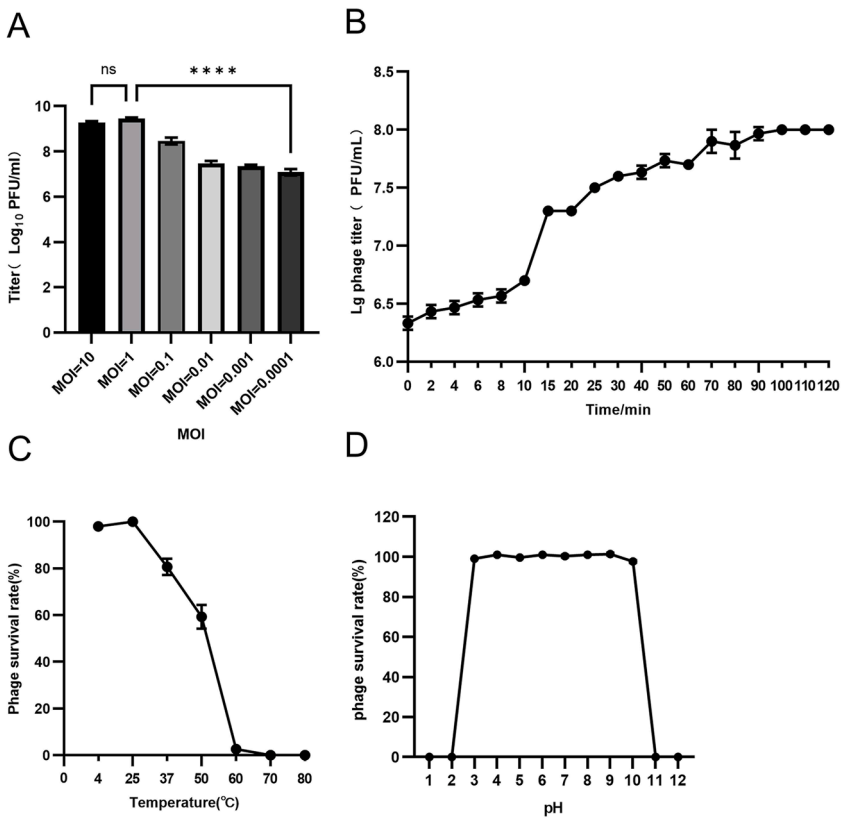

Fig. 2. Biological characterization of phage vB_Kp_Z1. **A** Determination of the optimal multiplicity of infection (MOI). Progeny phage titers were measured at different MOIs, and the optimal MOI was determined to be 1. **B** One-step growth curve. The latent period was approximately 10 min, and the phage titer reached a plateau at 100 min post-infection. **C** Thermal stability. Phage vB_Kp_Z1 was incubated at temperatures ranging from 4 °C to 80 °C for 1 h, and the remaining titers were determined by the double-layer agar method. **D** pH stability. Phage vB_Kp_Z1 was incubated at 25 °C for 1 h in buffers ranging from pH 1 to 12, and the remaining titers were determined by the double-layer agar method.

associated with codon usage adaptation or optimization of translational efficiency. The genetic map of phage vB_Kp_Z1 was constructed using Proksee (Fig. 3A). Analysis based on the PHACTS database predicted that vB_Kp_Z1 exhibits a lytic lifestyle, a feature that confers potential clinical application value. PhageScope analysis revealed no lysogeny-associated elements (integrases, recombinases, or repressors) within the vB_Kp_Z1 genome. Likewise, ABRicate detected no virulence factors or antibiotic resistance genes. Comparative genomic analysis demonstrated that vB_Kp_Z1 shows the highest sequence similarity to *Klebsiella* phage RCIP0053 (OR532847.1), with BLASTn alignment revealing 89% genome coverage and 97.07% nucleotide identity (Fig. 3B).

Proteome-based phylogenetic analysis using VIPtree showed that phage vB_Kp_Z1 clustered with members of the family *Autographiviridae* and is consistent with phages infecting hosts within the phylum *Pseudomonadota* (Supplementary Fig. S2A). Phylogenetic analysis based on the RNA polymerase major subunit further placed vB_Kp_Z1 within a well-supported clade comprising *Gajwadongvirus* phages (Supplementary Fig. S2B), supporting its taxonomic assignment to the genus *Gajwadongvirus* within the family *Autographiviridae* of the class *Caudoviricetes*.

To clarify its genomic relatedness, the twelve most closely related phage genomes were identified using BLASTn and subjected to genome-wide similarity analysis. Intergenomic similarities calculated using VIRIDIC showed that vB_Kp_Z1 shared the highest similarity with *Klebsiella* phage Roth32 (92.6%), while the minimum similarity among the analyzed phages was 71.8%, exceeding the 70% genus-level threshold (Fig. 4).

According to the current ICTV taxonomy (ICTV, https://ictv.global/taxonomy), three species are recognized within Gajwadongvirus: Gajwadongvirus ECBP5, Gajwadongvirus MR4, and Gajwadongvirus PP99. Based on the species demarcation criterion of intergenomic similarity >95%, vB_Kp_Z1 cannot be assigned to any currently recognized species, indicating that it represents a distinct species within this genus (Cai et al., 2022).

In vitro antibacterial and anti-biofilm activity

Phage vB_Kp_Z1 effectively inhibited the growth of *K. pneumoniae* strains KP1897 and KP177 *in vitro*. At an MOI of 1, phage-treated cultures exhibited significantly reduced OD_{600} values compared with SM buffer-treated controls. Growth suppression was evident within approximately 3 h for strain KP177 and 4.5 h for strain KP1897, consistent with the optimal MOI identified above (Fig. 5A).

To evaluate the anti-biofilm activity of phage vB_Kp_Z1, biofilm formation by *K. pneumoniae* strains was quantified at 24, 48, and 72 h under different multiplicities of infection (MOIs of 0.1, 1, and 10). The OD_{595} values of phage-treated groups were consistently significantly lower than those of the positive control at all time points, indicating effective inhibition of biofilm formation by vB_Kp_Z1. Notably, the most pronounced reduction in biofilm biomass at 24 h was observed at an MOI of 10, resulting in a 63% decrease. In contrast, at 48 and 72 h, the greatest inhibitory effect occurred at an MOI of 1, with biofilm biomass reductions of 44% and 28%, respectively (Fig. 5B; Supplementary Fig. S3).

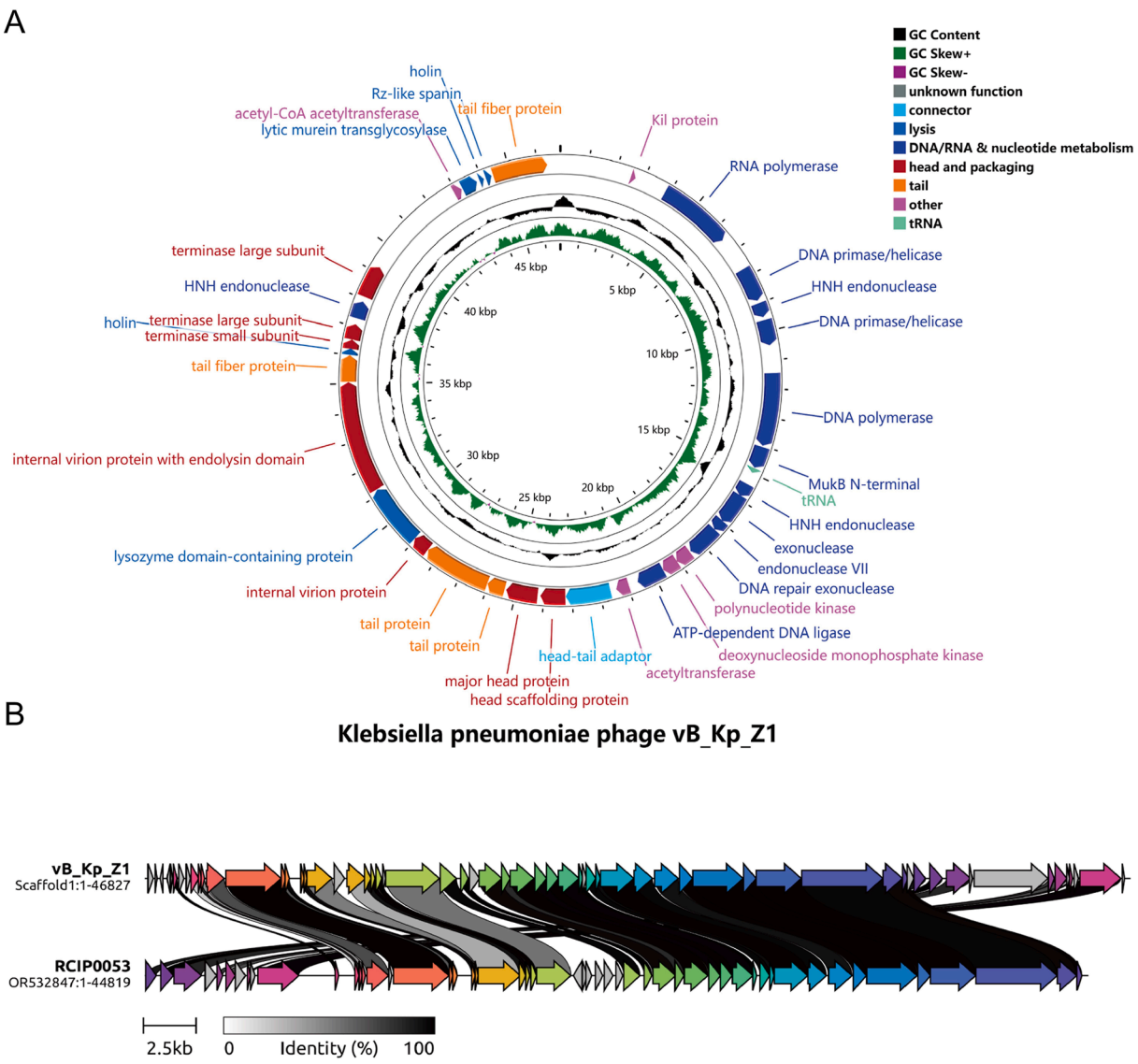

Fig. 3. Genome map and comparative genomic analysis of phage vB_Kp_Z1. **A** Circular genome map of phage vB_Kp_Z1 generated using Pharokka, showing GC content, GC skew, annotated functional proteins, and putative proteins. A total of 61 coding sequences (CDSs) were identified, including 34 with assigned functions and 27 hypothetical proteins. **B** Whole-genome comparison between phage vB_Kp_Z1 and the related phage RCIP0053 performed using Clinker, illustrating genome synteny.

Evaluation of phage protection

To assess the *in vivo* therapeutic efficacy of phage vB_Kp_Z1, murine intraperitoneal infection models were established using KP1897 and KP177, followed by phage treatment (Fig. 6A). All mice infected with KP1897 (Group 1) and KP177 (Group 3) and treated with PBS succumbed within 18 h post-infection. In contrast, phage administration conferred marked protection, with 100% survival observed in mice infected with KP1897 (Group 2) and 87.5% survival (7/8) in mice infected with KP177 (Group 4) (Fig. 6B).

During the first 24 h following infection, phage-treated mice exhibited transient clinical signs, including lethargy, reduced activity, huddling behavior, and ruffled fur. These symptoms gradually resolved after 24 h, and all surviving mice resumed normal feeding and drinking behaviors and survived for at least 7 days post-infection.

Bacterial burden analysis at 10 h post-infection revealed extensive systemic dissemination in control mice, with high colony-forming unit (CFU) counts detected in blood, lung, and liver tissues, with the highest bacterial loads observed in the liver. In contrast, mice receiving phage treatment exhibited significantly reduced bacterial loads in all examined tissues compared with the corresponding control groups, indicating effective bacterial clearance following phage therapy (Fig. 6C).

Histopathological analysis revealed the following findings (Fig. 6D): Group 1 exhibited hepatocellular vacuolar degeneration, marked sinusoidal congestion with dilation, and numerous congested blood vessels in the liver. Lung tissues showed mild but widespread thickening of alveolar walls, widespread congestion of alveolar wall capillaries, eosinophilic material within alveolar spaces, and occasional perivascular hemorrhage. In contrast, Group 2 displayed only mild vascular congestion in the liver, while eosinophilic material and exfoliated epithelial cells were observed in alveolar spaces together with mild interstitial vascular congestion in the lung, with no other significant abnormalities detected. Group 3 presented mild hepatocellular edema with pale and loosely arranged cytoplasm, occasional focal necrosis accompanied by nuclear fragmentation and structural disintegration, together with scattered lymphocytes and granulocytes. The lung tissues showed mild granulocyte infiltration in alveolar walls, slight thickening of alveolar walls, widened interalveolar septa, and narrowed alveolar spaces. In comparison, Group 4 demonstrated hepatocellular necrosis and inflammatory cell infiltration without significant congestion in the

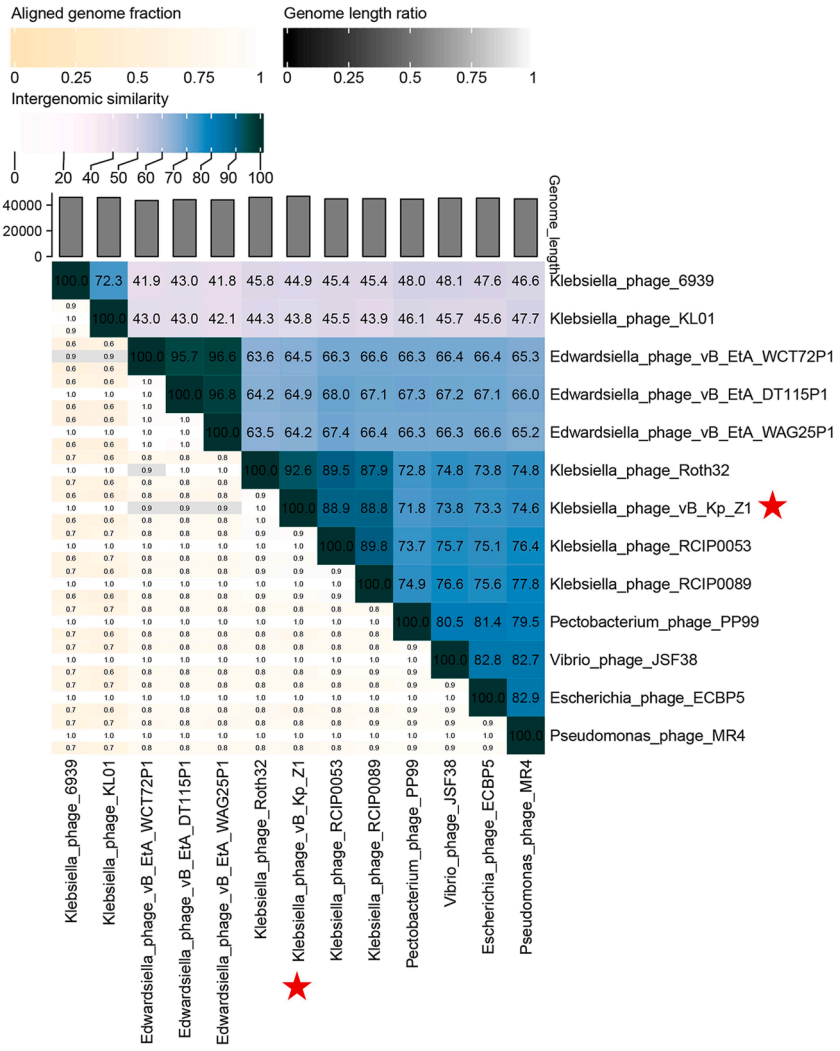

Fig. 4. Intergenomic similarity analysis of phage vB_Kp_Z1 using VIRIDIC. Heatmap showing pairwise intergenomic similarities between phage vB_Kp_Z1 and 12 closely related *K. pneumoniae* phages. Matrix values represent percentage similarities. Phage vB_Kp_Z1 is highlighted with a red star, and the color scale indicating similarity is shown on the right.

liver, as well as an increased extent of alveolar space narrowing in the lung, with no other notable differences observed.

To further quantify tissue injury, semi-quantitative histopathological scoring was performed (Fig. 6E). Mice in the PBS-treated groups exhibited significantly elevated liver and lung injury scores compared with the corresponding phage-treated groups. Phage administration markedly reduced the severity of tissue injury in both infection models, in agreement with the histopathological findings.

DISCUSSION

K. pneumoniae is a widespread opportunistic pathogen with zoonotic potential and represents a potential source of contamination in clinical settings, livestock production systems, and foods of animal origin (Monegro et al., 2025). The increasing prevalence of hypervirulent and multidrug-resistant strains has raised concerns regarding public health and food safety (Dong et al., 2022; Chen et al., 2025). In particular, the K1 serotype of *K. pneumoniae* is characterized by a dense capsular polysaccharide that promotes immune evasion and is strongly associated with invasive infections such as liver abscesses and meningitis (Huang et al., 2022). These challenges highlight the need for alternative antimicrobial strategies with high specificity, among which bacteriophages have gained increasing attention (Corbellino et al., 2020; Abbas et al., 2025; Lin et al., 2025).

In this study, we isolated the lytic phage vB_Kp_Z1 from hospital wastewater and evaluated its biological characteristics and antibacterial activity against K1 hypervirulent *K. pneumoniae*. Transmission electron microscopy revealed an icosahedral head with a short tail. The phage remained stable over a broad temperature range (4–50 °C) and across pH values of 3–11, suggesting potential compatibility with therapeutic applications. An MOI of 1 was sufficient to achieve effective bacterial inhibition at relatively low phage concentrations, which may reduce production costs and limit excessive phage exposure *in vivo*. One-step growth analysis demonstrated a short latent period of approximately 10 min and a strong lytic profile, reflecting high replication efficiency. Short latent periods combined with potent lytic activity are considered critical for rapid pathogen clearance (Shi et al., 2026), underscoring the therapeutic potential of vB_Kp_Z1. Host range analysis demonstrated that vB_Kp_Z1 exhibited lytic activity exclusively against K1 serotype *Klebsiella pneumoniae*, with no detectable activity toward non-K1 strains or other Enterobacteriaceae, indicating strict capsular type specificity for K1 strains.

Genomic characterization further supported the therapeutic suitability of vB_Kp_Z1. PHACTS analysis predicted a lytic lifestyle, and subsequent safety assessments confirmed the absence of lysogeny-associated elements, virulence factors, and antibiotic resistance genes. These results indicate that vB_Kp_Z1 is a strictly lytic phage incapable of chromosomal integration. Therefore, the risk of horizontal gene transfer

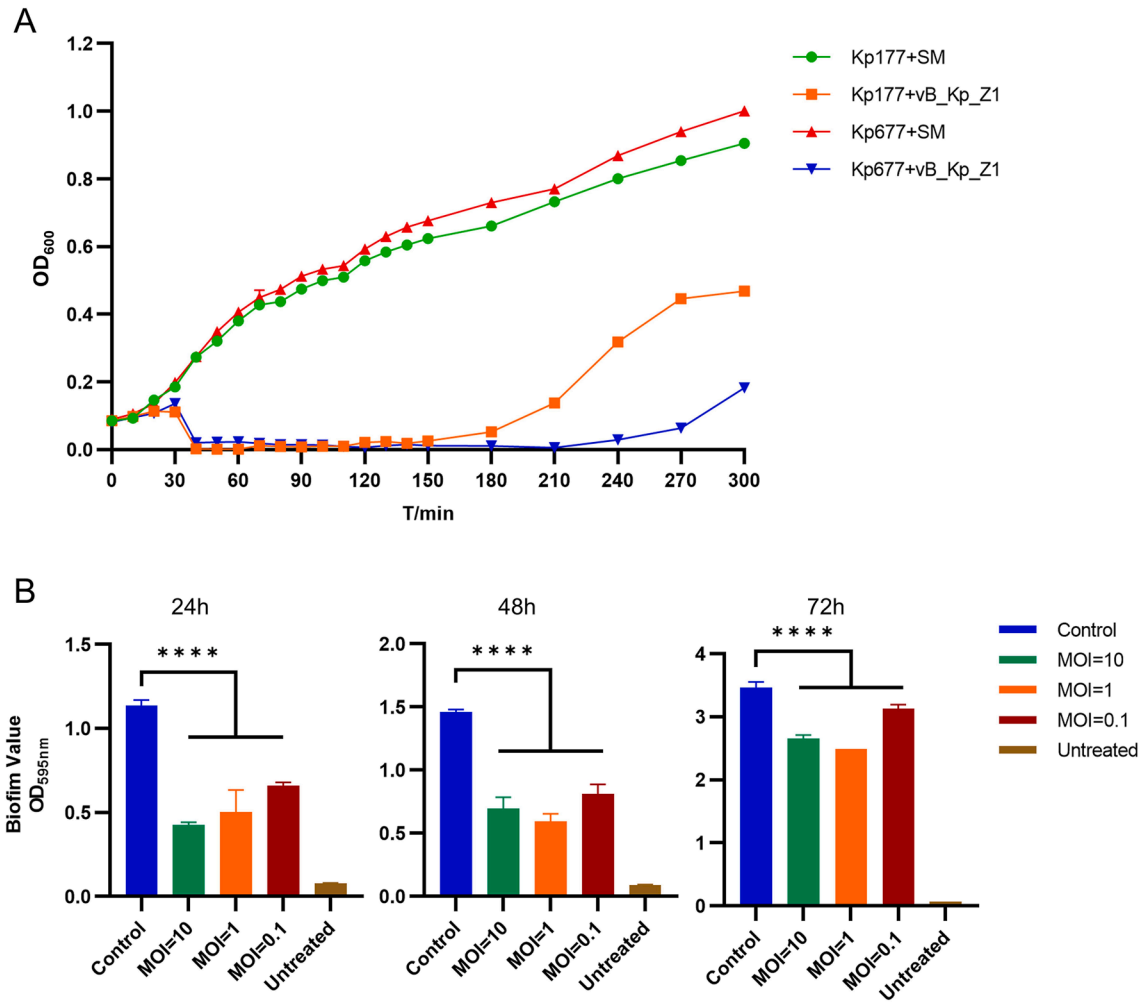

Fig. 5. Growth inhibition and antibiofilm activity of phage vB_Kp_Z1. **A** Growth curves of KP1897 and KP177 under SM buffer (control) and phage vB_Kp_Z1 treatment at a multiplicity of infection (MOI) of 1. Bacterial growth was monitored by measuring OD_{600} over time. **B** OD_{595} values of biofilms formed at 24 h, 48 h, and 72 h following treatment with phage vB_Kp_Z1 at multiplicity of infection (MOI) of 0.1, 1, and 10. Phage treatment reduced biofilm biomass compared with the positive control. Statistical significance was assessed by one-way ANOVA, and asterisks indicate significant differences (*$P < 0.05$; **$P < 0.01$; ***$P < 0.001$; ****$P < 0.0001$).

via lysogenic conversion is negligible, supporting a favorable safety profile. Phylogenetic analyses placed vB_Kp_Z1 within the genus Gajwadongvirus of the family Autographiviridae, while its relatively low nucleotide similarity to previously described phages suggests that it represents a distinct species (Adriaenssens and Brister, 2017). Notably, phages within the Autographiviridae are known to encode their own RNA polymerase, a feature associated with rapid transcription and replication, consistent with the efficient lytic dynamics observed in this study (Boeckman et al., 2022). Collectively, these biological and genomic characteristics suggest the potential of vB_Kp_Z1 as a promising candidate for further evaluation in phage-based interventions targeting hvKP infections.

Functionally, vB_Kp_Z1 exhibited marked antibacterial activity against two K1-type hypervirulent *K. pneumoniae* strains under planktonic conditions, with sustained reductions in bacterial growth observed. Differences in the extent and persistence of bacterial growth suppression between the two strains suggest host-dependent variation in phage efficacy, most likely reflecting differences in phage-receptor compatibility and adsorption efficiency (Chen et al., 2024). In addition, vB_Kp_Z1 inhibited biofilm formation to a notable extent at all tested time points, with the most pronounced effect observed during the early stages of biofilm development. Although anti-biofilm efficacy decreased over time, all tested phage doses resulted in significant biomass reduction, with an MOI of 1 showing the most consistent overall activity.

The *in vivo* efficacy of vB_Kp_Z1 was assessed using mouse intraperitoneal infection models challenged with K1-type hypervirulent *K. pneumoniae*. Infection with hvKP strains KP1897 and KP177 led to rapid disease progression, with all untreated mice dying within 12 h, consistent with the strong virulence and systemic dissemination reported for K1 hvKP in animal models. Phage treatment significantly improved survival and reduced bacterial loads in blood and major organs, in agreement with previous studies evaluating phage therapy in mouse hvKP infections (Li et al., 2024a,b). Marked reductions in bacterial burden were observed in both the liver and lungs, which represent key target organs during K1-type hvKP infection. Notably, K1 *K. pneumoniae* has been strongly associated with invasive syndromes involving hepatic infection (Psonis et al., 2022), whereas experimental models evaluating phage-based interventions against K1-associated liver infection are relatively limited. The present findings therefore provide *in vivo* evidence supporting the feasibility of phage therapy for controlling of hepatic hvKP infection.

Phage vB_Kp_Z1 enhanced survival and reduced bacterial loads in mice infected with KP1897 or KP177, though survival outcomes differed

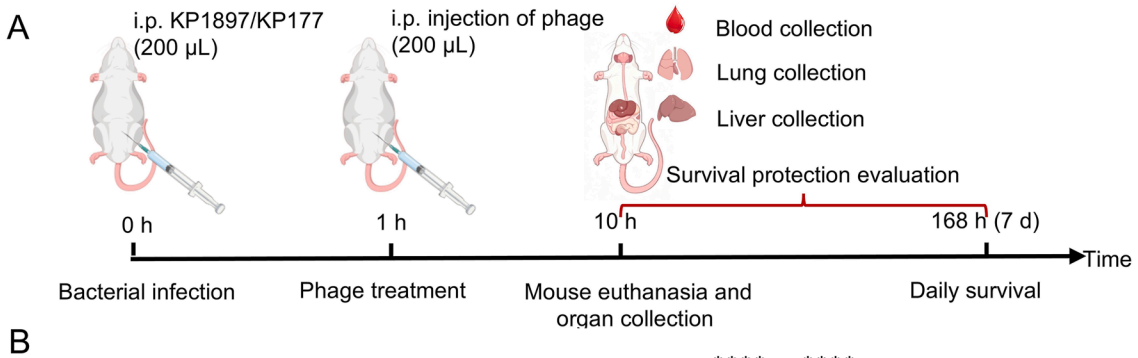

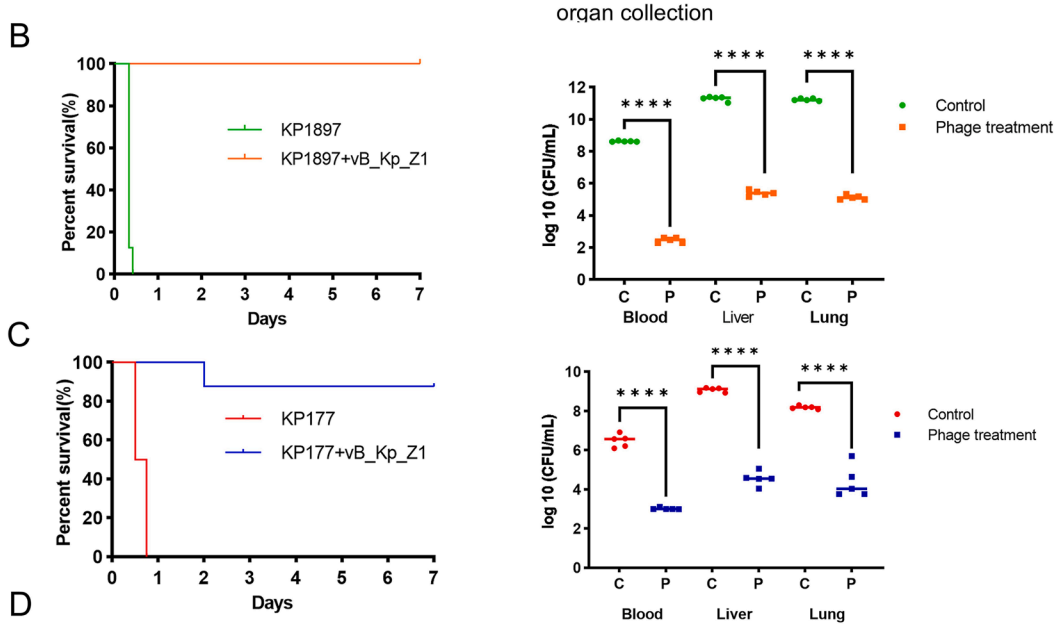

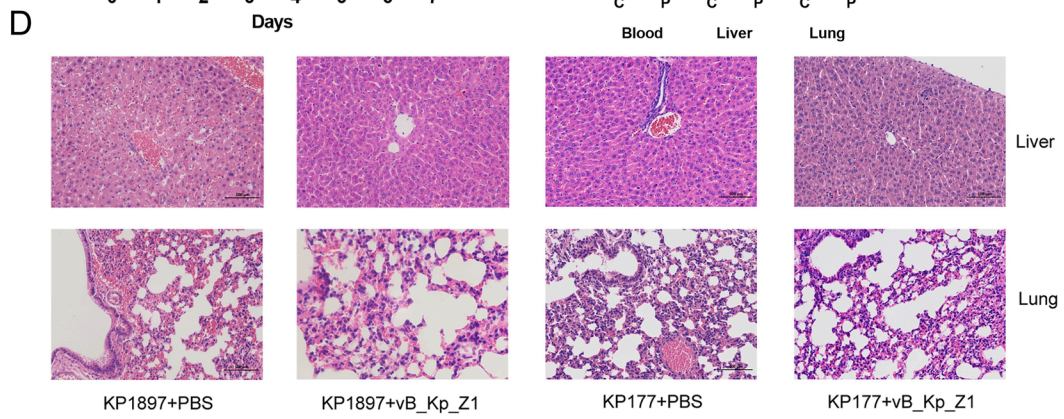

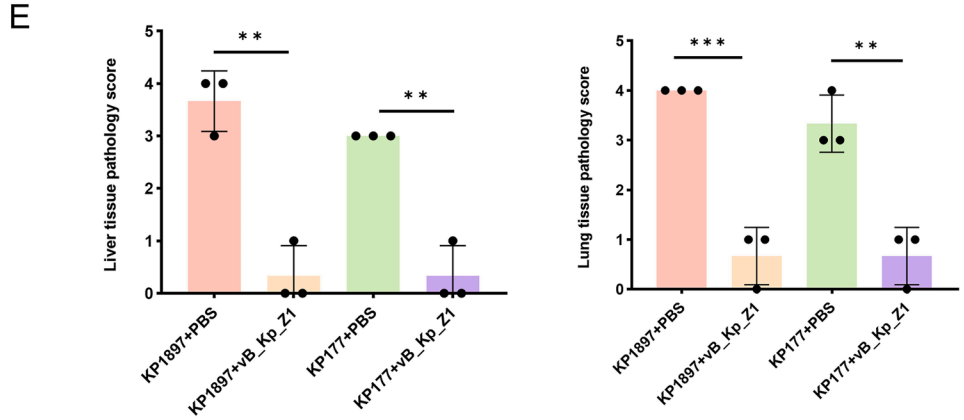

(caption on next page)

Fig. 6. Therapeutic efficacy of phage vB_Kp_Z1 in a mouse model of *Klebsiella pneumoniae* infection, with pathological evaluation of liver and lung injury. **A** Experimental design. Mice were intraperitoneally challenged with *K. pneumoniae* (KP1897 or KP177) at 0 h, followed by administration of phage vB_Kp_Z1 or PBS at 1 h. Blood, lung, and liver samples ($n = 5$) were collected at 10 h, and the remaining mice ($n = 8$) were monitored for survival up to 168 h. **B** Survival of mice infected with KP1897 and treated with phage vB_Kp_Z1 or control. Survival of mice infected with KP177 and treated with phage vB_Kp_Z1 or control. **C** Bacterial loads in blood, liver, and lung tissues of mice infected with KP1897 (green symbols) or KP177 (blue symbols), comparing phage-treated and control groups. Statistical significance was assessed by unpaired *t*-test (****$P < 0.0001$). **D** Representative H&E-stained liver and lung sections from the four experimental groups. Scale bar, 100 μm. **E** Semi-quantitative pathological scores of liver and lung tissues. Statistical significance was assessed by unpaired *t*-test (****$P < 0.0001$).

between strains, indicating variation in phage susceptibility. Although complete bacterial clearance was not achieved, no overt expansion of phage-resistant populations was observed, consistent with reports that resistance *in vivo* may incur fitness costs (Li et al., 2024a,b). Histopathology further showed attenuated organ injury in treated mice, which is consistent with both the bacterial burden data and the semi-quantitative pathological scoring results. It is important to note that this study only assessed short-term efficacy in an acute model and did not examine longer infection dynamics or possible intracellular bacterial persistence under phage treatment, a phenomenon linked to resistance development in hvKP (Chen et al., 2025). Taken together, these results suggest that vB_Kp_Z1 provides substantial *in vivo* protection against K1 hvKP from different origins, supporting its therapeutic potential while highlighting the need to better understand host-related constraints on phage activity.

CONCLUSIONS

In this study, we isolated a novel lytic bacteriophage, vB_Kp_Z1, that exhibits strict capsular serotype specificity for K1-type *Klebsiella pneumoniae*. vB_Kp_Z1 efficiently inhibited planktonic growth and biofilm formation of K1 strains *in vitro*. Genomic analysis revealed no lysogeny-associated elements, virulence factors, or antibiotic resistance genes, suggesting that vB_Kp_Z1 has a favorable biosafety profile. In a mouse model of intraperitoneal infection with hypervirulent K1-type *K. pneumoniae*, phage treatment significantly improved survival and reduced bacterial burdens in the blood, liver, and lungs. This effect was accompanied by attenuated histopathological injury, consistent with the observed reduction in bacterial load. Given the strong association of K1 serotype with invasive disease and the limited availability of well-characterized K1-specific phages, these findings provide *in vivo* evidence supporting the feasibility of capsular serotype-targeted phage therapy against hypervirulent K1 infections and offer an experimental basis for further investigation of targeted phage-host interactions within this clinically important lineage.

MATERIALS AND METHODS

Bacterial strains and growth conditions

The *Klebsiella pneumoniae* strain KP1897, isolated from a meat pigeon in Xinjiang, China, was used for bacteriophage isolation and propagation. A human-derived *K. pneumoniae* strain KP177, kindly provided by Prof. Hong Du, was included in mouse infection experiments to represent a clinically relevant K1 isolate. Source and capsular serotype information for these strains and other isolates used in host range analysis are provided in Table 1. KP177 was selected for *in vivo* experiments based on its phenotypic characteristics and antimicrobial susceptibility profile, and hypermucoviscosity was assessed using the string test. Antimicrobial susceptibility was determined by measuring minimum inhibitory concentrations (MICs) according to the CLSI M100 ED33-2023 guidelines, and the results for strains used in mouse experiments are summarized in Supplementary Table S1. All bacterial isolates were routinely cultured in Luria-Bertani (LB) broth (Thermo Fisher Scientific, Waltham, MA, USA) at 37 °C with shaking at 180 rpm. For animal infection and *in vitro* assays, bacterial suspensions were prepared by diluting in sterile phosphate-buffered saline (PBS; 0.1 mol/L Na_2HPO_4, 0.15 mol/L NaCl, pH 7.4) to the desired concentrations.

Phage isolation and purification

Phage vB_Kp_Z1 was isolated from mixed hospital sewage collected in Jiangsu Province, China, using the clinical *K. pneumoniae* strain KP1897 as the host bacterium. Briefly, 10 mL of sewage was centrifuged at 5000×*g* for 10 min, and the supernatant was filtered through a 0.22 μm membrane filter (Millipore, Burlington, MA, USA). The filtrate was mixed with 20 mL of LB broth, inoculated with 200 μL of an exponentially growing culture of strain KP1897, and incubated at 37 °C with shaking at 180 rpm for 12 h to enrich phages. The culture was then centrifuged and filtered again through a 0.22 μm membrane filter, and the resulting filtrate was serially diluted and plated using the double-layer agar method to obtain individual plaques. Well-isolated plaques were picked and resuspended in SM buffer (20 mM Tris-HCl, 10 mM $MgSO_4$, 10 mM $CaCl_2$, 100 mM NaCl, pH 7.5), and plaque purification was repeated at least three times until uniform plaque morphology was obtained. The purified phage vB_Kp_Z1 was stored at 4 °C for subsequent experiments.

Host range

The host range of phage vB_Kp_Z1 was assessed using spot assays and double-layer agar plaque assays as previously described (Li et al., 2020). A total of 61 *Klebsiella pneumoniae* strains representing 26 distinct capsular serotypes were included. In addition, 10 non-*K. pneumoniae* Enterobacteriaceae strains, including *Escherichia coli*, *Salmonella* spp., and *Yersinia enterocolitica*, were tested to evaluate the interspecies specificity of the phage (Table 1). For spot assays, 100 μL of each bacterial culture grown to the logarithmic phase (OD_{600} = 0.4–0.6) was spread onto LB agar plates, and 5 μL of phage suspension (1×10^9 PFU/mL) was spotted onto the bacterial lawn, with sterile PBS used as a negative control. For double-layer agar plaque assays, 100 μL of bacterial culture was mixed with 100 μL of phage suspension and overlaid onto LB agar plates containing molten soft agar. Plates were incubated at 37 °C for 12 h, and plaques were assessed for phage lytic activity and host specificity.

Transmission electron microscopy (TEM)

To characterize the morphology of phage vB_Kp_Z1, TEM was performed. Purified phage suspensions were applied to carbon-coated copper grids and allowed to adsorb for several minutes. Excess liquid was removed, and the grids were negatively stained with 2% (w/v) phosphotungstic acid (PTA) (Sigma-Aldrich, St. Louis, MO, USA). After air-drying for 30 min at room temperature, phage particles were observed using a Hitachi H-7700 TEM (Hitachi, Tokyo, Japan). Particle dimensions were measured from TEM images using ImageJ (NIH, Bethesda, MD, USA).

Optimal multiplicity of infection and one-step growth curve

The MOI of phage vB_Kp_Z1 was determined using KP1897 as the host bacterium. Exponentially growing bacterial cultures (5×10^8 CFU/mL; OD_{600} = 0.5) were mixed with phage suspensions at MOIs of 10, 1, 0.1, 0.01, 0.001, and 0.0001. The mixtures were then incubated at 37 °C with shaking at 180 rpm for 12 h. Following incubation, the cultures were centrifuged at 5000×*g* for 5 min, and the supernatants were collected,

Table 1
Host range of vB_Kp_Z1.

Bacteria	Source	Year	KL/K type	vB_Kp_Z1 Plaques
KP55	Human	2019	K1	+
KP177	Human	2020	K1	+
KP670	Pigeon	2023	K1	+
KP706	Human	2023	K1	+
KP813	Human	2023	K1	+
KP840	Human	2023	K1	+
KP871	Human	2023	K1	+
KP923	Human	2023	K1	+
KP1007	Human	2024	K1	+
KP1181	Cow	2024	K1	+
KP1182	Cow	2024	K1	+
KP1184	Cow	2024	K1	+
KP1186	Cow	2024	K1	+
KP1626	Human	2025	K1	+
KP1630	Human	2025	K1	+
KP1633	Human	2025	K1	+
KP1634	Cow	2025	K1	+
KP1694	Cow	2025	K1	+
KP1722	Cow	2025	K1	+
KP1897	Pigeon	2023	K1	+
KP125	Human	2020	K2	–
KP264	Cow	2021	K2	–
KP1128	Human	2024	K2	–
KP73	Cow	2019	K3	–
KP74	Cow	2019	K3	–
KP796	Human	2023	K3	–
KP84	Cow	2019	K5	–
KP858	Human	2023	K5	–
KP1140	Human	2024	K5	–
KP290	Cow	2021	K7	–
KP485	Human	2022	K15	–
KP903	Human	2023	K19	–
KP911	Human	2023	K19	–
KP1250	Pig	2025	K19	–
KP300	Cow	2021	K20	–
KP1133	Human	2024	K20	–
KP315	Cow	2021	K21	–
KP1423	Pig	2025	K23	–
KP883	Human	2023	K24	–
KP1424	Pig	2025	K28	–
KP153	Human	2020	K47	–
KP253	Cow	2021	K47	–
KP637	Human	2023	K51	–
KP86	Cow	2019	K54	–
KP820	Human	2023	K54	–
KP947	Human	2023	K57	–
KP1146	Cow	2024	K57	–
KP1180	Pig	2024	K57	–
KP912	Human	2023	K64	–
KP935	Human	2023	K64	–
KP697	Human	2023	KL103	–
KP701	Human	2023	KL103	–
KP801	Cow	2023	KL105	–
KP1383	Pig	2024	KL109	–
KP345	Human	2021	KL110	–
KP448	Human	2022	KL123	–
KP874	Human	2023	KL128	–
KP52	Human	2019	KL136	–
KP890	Human	2023	KL136	–
KP1149	Pig	2024	KL148	–
KP1220	Pig	2024	KL149	–
EC618	Cow	2020	O2	–
EC693	Duck	2020	O78	–
EC274	Ovine	2019	O157	–
EC275	Ovine	2019	O157	–
SA322	Chicken	2021	–	–
SA610	Ovine	2022	–	–
SA623	Ovine	2022	–	–
YE030	Ovine	2022	–	–
YE050	Pig	2022	O3	–
YE056	Pig	2022	O8	–

+, clear lytic zones/plaques observed; –, no lytic activity detected.

serially diluted, and titrated by the double-layer agar method to determine phage yields. All assays were performed independently in triplicate.

A one-step growth experiment was conducted to assess the replication dynamics of vB_Kp_Z1. 1 mL of phage particles (5×10^9 PFU/mL) was mixed with host bacteria (5×10^8 CFU/mL) at an MOI of 1 and allowed to adsorb at 37 °C for 5 min. The mixture was then centrifuged at 5000×*g* for 2 min at 4 °C to remove unadsorbed phages. The bacterial pellet was washed three times with PBS, resuspended in 10 mL LB, and incubated at 37 °C with shaking at 180 rpm for 2 h. Samples were collected at regular intervals (every 2 min during the first 10 min, every 5 min from 10 to 30 min, and every 10 min thereafter), and phage titers were determined using the double-layer agar method. The experiment was repeated independently in triplicate.

Temperature and pH stability

The stability of phage vB_Kp_Z1 under different temperature and pH conditions was examined. For temperature stability, 100 μL of phage suspension with a titer of 1×10^9 PFU/mL was mixed with 900 μL of SM buffer and incubated at 4, 25, 37, 50, 60, 70, and 80 °C for 1 h, after which residual phage titers were determined using the double-layer agar method. For pH stability, 100 μL of phage suspension with a titer of 1×10^9 PFU/mL was mixed with 900 μL of SM buffer adjusted to pH 1–12 and incubated at 25 °C for 1 h, and phage titers were then determined using the double-layer agar method. All experiments were performed independently in triplicate.

Phage DNA extraction and whole genome sequencing

Phage stocks of vB_Kp_Z1 (1.0×10^9 PFU/mL) were prepared using the double-layer agar method. Phage genomic DNA was extracted according to the manufacturer's instructions using a λ phage genomic DNA extraction kit (Zomanbio, Beijing, China). Sequencing was performed using the Illumina Nova X plus system (Illumina, San Diego, CA, USA) and carried out by Novogene Bioinformatics Technology Co., Ltd. (Novogene, Beijing, China).

Phage genome analysis

The whole genome sequence of phage vB_Kp_Z1 was deposited in the NCBI database under accession number PQ308734.1. Genome annotation was performed using Pharokka v1.7.3 (https://github.com/gbouras13/pharokka). Functional prediction of annotated genes was carried out using the online BLASTp tool (http://www.ncbi.nlm.nih.gov/BLAST). The lifestyle of the phage was predicted using the PHACTS database (http://www.phantome.org/PHACTS/) (McNair et al., 2012). To evaluate the genomic safety of phage vB_Kp_Z1, PhageScope (https://phagescope.deepomics.org/) was used to detect lysogeny-associated elements (e.g., integrases, recombinases, and repressors), and ABRicate v1.0.1 (https://github.com/tseemann/abricate) was used to identify potential virulence factors and antimicrobial resistance genes. Transfer RNA (tRNA) genes were detected using tRNAscan-SE 2.0 (http://lowelab.ucsc.edu/tRNAscan-SE/) (Chan et al., 2021).

The assembled genome sequence was further analyzed using the BLASTn algorithm (https://blast.ncbi.nlm.nih.gov/Blast.cgi) to assess genomic novelty. The twelve most closely related phage genomes were identified based on BLASTn results, and pairwise intergenomic similarity at the nucleotide level was performed using VIRIDIC (Moraru et al., 2020). Comparative genomic analysis and visualization were conducted using Clinker v0.0.28 (Gilchrist and Chooi, 2021). A phage proteomic tree was constructed using the Viral Proteome Tree Server (VIPTree) (http://www.genome.jp/viptree/). Phylogenetic analysis was performed based on the amino acid sequences of the terminase large

subunit retrieved from related phages in the NCBI database. Multiple sequence alignment was conducted using Clustal W, and a phylogenetic tree was constructed using MEGA X with the Neighbor-Joining method and 1000 bootstrap replicates (Kumar et al., 2018).

Antibacterial activity of vB_Kp_Z1 *in vitro*

5 mL of phage vB_Kp_Z1 was separately mixed with 5 mL cultures of KP1897 and KP177, each adjusted to 1×10^8 CFU/mL, to obtain a multiplicity of infection of 1 in 20 mL LB medium. The co-cultures were incubated at 37 °C with shaking at 180 rpm. For each strain, a corresponding control group consisting of the bacterial culture treated with sterile SM buffer was maintained under identical conditions. Bacterial growth was monitored by measuring OD_{600} at 10 min intervals for the first 2.5 h and at 30 min intervals for the subsequent 2.5 h. All experiments were performed independently in triplicate.

Inhibition of biofilms by vB_Kp_Z1 *in vitro*

The anti-biofilm activity of phage vB_Kp_Z1 was evaluated using 96-well flat-bottom polystyrene microplates (Corning Incorporated, Corning, NY, USA). KP1897 was adjusted to a concentration of 1×10^8 CFU/mL and used for biofilm formation. Five experimental groups were established as follows: a positive control group containing 100 μL of KP1897 bacterial suspension and 100 μL of fresh LB medium; phage treatment groups at multiplicities of infection of 10, 1, and 0.1, each containing 100 μL of KP1897 bacterial suspension mixed with 100 μL of vB_Kp_Z1 suspension at concentrations of 1×10^9, 1×10^8, and 1×10^7 PFU/mL, respectively; and a negative control group containing 200 μL of LB medium. Plates were incubated at 37 °C for 24, 48, and 72 h.

After incubation, the culture medium was gently removed from each well. The wells were washed three times with 200 μL of sterile phosphate-buffered saline, with the liquid discarded after each wash. Subsequently, 100 μL of methanol was added to each well for fixation and incubated for 15 min at room temperature, after which the methanol was removed. The fixed biofilms were stained with 100 μL of 1% crystal violet solution (Sigma-Aldrich, St. Louis, MO, USA) for 10 min. Excess stain was removed by rinsing the wells with running water until no visible dye remained. The bound crystal violet was then solubilized by adding 33% acetic acid (Sigma-Aldrich, St. Louis, MO, USA) and incubating the plates at 37 °C for 30 min, as previously described (Li et al., 2024a,b). Biofilm biomass was quantified by measuring the absorbance at 595 nm using a microplate reader (BioTek, Winooski, VT, USA). All experiments were performed independently in triplicate.

Mouse infection and treatment

The animal experiment was conducted according to previously described methods (Ma et al., 2023). Four-week-old female BALB/c mice were obtained from Jiangsu Qinglongshan Biotechnology Co., Ltd. (Nanjing, China) and randomly assigned to four groups based on infection strain and treatment. The groups were defined as follows: Group 1, positive control (KP1897-infected mice administered 200 μL PBS at 1 h post-infection); Group 2, phage treatment (KP1897-infected mice receiving phage at 1 h post-infection); Group 3, positive control (KP177-infected mice administered 200 μL PBS at 1 h post-infection); Group 4, phage treatment (KP177-infected mice receiving phage at 1 h post-infection). Each group consisted of thirteen animals, of which eight were monitored for survival, while the remaining five were euthanized at predetermined time points for bacterial load determination and histopathological analysis. All mice were maintained under standard housing conditions with ad libitum access to food and water, and all procedures were performed to minimize distress.

Infection was established via intraperitoneal injection with KP1897 at 1×10^7 CFU and KP177 at 5×10^7 CFU, each delivered in 200 μL of suspension. One hour later, mice in the treatment groups received 200 μL of phage vB_Kp_Z1 at a dose of 1×10^9 PFU, whereas control groups received an equal volume of sterile PBS. Survival was monitored daily for seven days following treatment.

Ten hours after infection, five mice from each group were euthanized by cervical dislocation. Blood, lung, and liver samples were collected to assess bacterial loads. Blood was obtained from the retro-orbital venous plexus, and lung and liver tissues were homogenized, serially diluted, and plated for viable bacterial enumeration. For histopathological evaluation, lung and liver samples were fixed in 4% paraformaldehyde, processed using standard dehydration and paraffin-embedding procedures, and stained with hematoxylin and eosin (H&E) to examine tissue morphology and pathological alterations.

Histopathological evaluation and scoring

Histopathological changes in liver and lung tissues were evaluated using a semi-quantitative scoring system adapted from previously described methods (Zeng et al., 2021; Blot et al., 2025) and modified to reflect the pathological features observed in this study. Tissue sections were scored on a scale from 0 to 4. All slides were assessed independently by three blinded observers, and the mean score was used for statistical analysis.

Liver injury was evaluated based on inflammatory cell infiltration, hepatocellular degeneration and necrosis, sinusoidal congestion or hemorrhage, and microabscess formation. Lung injury was assessed based on inflammatory cell infiltration, alveolar septal thickening, alveolar exudation, hemorrhage or edema, and consolidation. Scores were defined as follows: 0, no or minimal lesions; 1, mild focal lesions (<25% of the section); 2, moderate localized lesions (25–50% of the section); 3, widespread or locally severe lesions (50–75% of the section); 4, extensive and severe lesions (>75% of the section).

Statistical analysis

Statistical analyses were performed using GraphPad Prism 9.5. Data are presented as mean ± SD. Differences among multiple groups were analyzed using one-way ANOVA, followed by appropriate post hoc tests. Survival was analyzed using the Kaplan–Meier method with the log-rank (Mantel–Cox) test. Two-group comparisons were performed using an unpaired two-tailed Student's t-test. A $P < 0.05$ was considered statistically significant.

DATA AVAILABILITY

Data will be made available on request. All data and sequences for this article are available on the Science Data Bank: 10.57760/sciencedb.v.00025.

ETHICS STATEMENT

This study was conducted in accordance with relevant ethical regulations and was approved by the Institutional Review Boards of Zhangjiagang Hospital Affiliated to Soochow University and the Second Affiliated Hospital of Soochow University. Clinical isolates were collected retrospectively, and no identifiable patient information was involved; therefore, informed consent was waived by the Institutional Review Boards.

All animal experiments were approved by the Experimental Animal Welfare and Ethics Committee of Nanjing Agricultural University (NJAU.No20260116012) and were conducted in accordance with the relevant Animal Welfare guidelines.

AUTHOR CONTRIBUTIONS

Xiaona Yan: conceptualization, data curation, formal analysis, validation, investigation, writing original draft, writing-review and editing. Mengmeng Su: data curation, visualization. Sixiang Xu: methodology. Xiangkuan Zheng: formal analysis. Xiaoyue Li: investigation. Peifan Liu: investigation. Yilin Fang: methodology. Libin Tan: methodology. Long Chen: resources. Hong Du: resources. Panpan Tong: resources. Yuxia Zhang: resources. QinghaiRen: resources, supervision. Wei Zhang: funding acquisition, resources, supervision, project administration.

CONFLICT OF INTEREST

The authors declare no potential conflicts of interest.

ACKNOWLEDGEMENTS

This study was supported by the Research and Development of Artificial Intelligence Diagnosis and Ecological Prevention Technologies for Major Bacterial Diseases in Large-Scale Pig Farms in Xinjiang (Project Number: 2026LQ03001), the Integration and Application of AI-Based Real-Time Diagnosis and Ecological Control Technologies for Animal Bacterial Diseases (Supported by the "Fundamental Research Funds for Central Universities"), the Key Research and Development Program of Ningxia Hui Autonomous Region (Grant No.2025BBF02009), the Key Research Project of Hainan Province: Rapid Diagnosis and Prevention Strategies for Acute Death Syndrome in Babylonia areolata (Project Number: ZDYF2025XDNY123), and the NHC Key Laboratory of Enteric Pathogenic Microbiology (Jiangsu Provincial Center for Disease Control and Prevention) (No. EM202303).

APPENDIX A. SUPPLEMENTARY DATA

Supplementary data to this article can be found online at https://doi.org/10.1016/j.virs.2026.06.003.

REFERENCES

Abbas, S., Kanwar, R., Ullah, K., Kanwal, R., Tajamal, M., Aslam, M.A., Ahmad, A., Qadeer, A., Huang, H., Chen, C., 2025. Bacteriophage therapy: a possible alternative therapy against antibiotic-resistant strains of *Klebsiella pneumoniae*. Front. Microbiol. 16, 1443430.

Adriaenssens, E., Brister, J.R., 2017. How to name and classify your phage: an informal guide. Viruses 9, 70.

Agyeman, A.A., Bergen, P.J., Rao, G.G., Nation, R.L., Landersdorfer, C.B., 2020. A systematic review and meta-analysis of treatment outcomes following antibiotic therapy among patients with carbapenem-resistant *Klebsiella pneumoniae* infections. Int. J. Antimicrob. Agents 55, 105833.

Blot, M., Léopold, V., de Beer, R., Florquin, S., Butler, J.M., Van't Veer, C., de Vos, A.F., van der Poll, T., 2025. The Sirt1 activator SRT1720 mitigates human monocyte activation and improves outcome during Gram-negative pneumosepsis in mice. Int. J. Mol. Sci. 26, 9309.

Boeckman, J., Korn, A., Yao, G., Ravindran, A., Gonzalez, C., Gill, J., 2022. Sheep in wolves' clothing: temperate T7-like bacteriophages and the origins of the Autographiviridae. Virology 568, 86–100.

Cai, R., Li, D., Lin, W., Qin, W., Pan, L., Wang, F., Qian, M., Liu, W., Zhou, Q., Zhou, C., Tong, Y., 2022. Genome sequence of the novel freshwater Microcystis cyanophage Mwe-Yong1112-1. Arch. Virol. 167, 2371–2376.

Chan, P.P., Lin, B.Y., Mak, A.J., Lowe, T.M., 2021. tRNAscan-SE 2.0: improved detection and functional classification of transfer RNA genes. Nucleic Acids Res. 49, 9077–9096.

Chen, H., Sun, Y., Huang, Z., Zhao, D., Kong, J., Chen, H., Zhou, C., Zhou, T., 2025. Evolving strategies of intracellular Hypervirulent *Klebsiella pneumoniae* during phage therapy: reducing host autophagy and inflammation. Virulence 16, 2600148.

Chen, J., Hou, Y., Shi, J., Gao, X., Liang, G., 2025. Mortality risk of carbapenem-resistant hypervirulent *Klebsiella pneumoniae* vs. classical CR-KP: a systematic review and meta-analysis. Front. Public Health 13, 1680292.

Chen, Q., Zhang, F., Bai, J., Che, Q., Xiang, L., Zhang, Z., Wang, Y., Sj Ling, S., Martín-Rodríguez, A.J., Zhu, B., Fu, L., Zhou, Y., 2024. Bacteriophage-resistant carbapenem-resistant *Klebsiella pneumoniae* shows reduced antibiotic resistance and virulence. Int. J. Antimicrob. Agents 64, 107221.

Choby, J.E., Howard-Anderson, J., Weiss, D.S., 2020. Hypervirulent *Klebsiella pneumoniae* - clinical and molecular perspectives. J. Intern. Med. 287, 283–300.

Corbellino, M., Kieffer, N., Kutateladze, M., Balarjishvili, N., Leshkasheli, L., Askilashvili, L., Tsertsvadze, G., Rimoldi, S.G., Nizharadze, D., Hoyle, N., Nadareishvili, L., Antinori, S., Pagani, C., Scorza, D.G., Romanò, A.L.L., Ardizzone, S., Danelli, P., Gismondo, M.R., Galli, M., Nordmann, P., Poirel, L., 2020. Eradication of a multidrug-resistant, carbapenemase-producing *Klebsiella pneumoniae* isolate following oral and intra-rectal therapy with a custom made, lytic bacteriophage preparation. Clin. Infect. Dis. 70, 1998–2001.

Ding, J., Yan, W., Zheng, R., Ma, M., Jiang, L., 2025. Combating *Klebsiella pneumoniae*: from antimicrobial resistance mechanisms to phage-based combination therapies. Front. Cell. Infect. Microbiol. 15, 1691215.

Dong, N., Yang, X., Chan, E.W., Zhang, R., Chen, S., 2022. Klebsiella species: taxonomy, hypervirulence and multidrug resistance. EBioMedicine 79, 103998.

Fang, Y., Zhong, Q., Chen, Y., Hang, Y., Fang, X., Xiao, Y., Cao, X., Zhu, H., Luo, H., Peng, S., Gu, S., Li, F., Zhu, J., Xiong, J., Hu, L., 2023. Ceftazidime/Avibactam, polymyxin or tigecycline as a rescue strategy for the treatment of carbapenem-resistant *Klebsiella pneumoniae* in bloodstream infection: a retrospective cohort study. Infect. Drug Resist. 16, 2963–2971.

Gilchrist, C.L.M., Chooi, Y., 2021. Clinker & clustermap.js: automatic generation of gene cluster comparison figures. Bioinformatics 37, 2473–2475.

Gradisteanu Pircalabioru, G., Popa, L.I., Marutescu, L., Gheorghe, I., Popa, M., Czobor Barbu, I., Cristescu, R., Chifiriuc, M., 2021. Bacteriocins in the era of antibiotic resistance: rising to the challenge. Pharmaceutics 13, 196.

Hsu, C., Lin, T., Chen, Y., Chou, H., Wang, J., 2011. The role of *Klebsiella pneumoniae* rmpA in capsular polysaccharide synthesis and virulence revisited. Microbiology 157, 3446–3457.

Huang, X., Li, X., An, H., Wang, J., Ding, M., Wang, L., Li, L., Ji, Q., Qu, F., Wang, H., Xu, Y., Lu, X., He, Y., Zhang, J., 2022. Capsule type defines the capability of *Klebsiella pneumoniae* in evading Kupffer cell capture in the liver. PLoS Pathog. 18, e1010693.

Jiao, S., Wang, X., Wang, J., Liu, Y., Zhang, L., Peng, X., Song, J., Wang, C., Zhang, W., Li, X., 2025. Phage vB_KpnM_JYSS3 encodes a novel polysaccharide depolymerase that exhibits specific activity against K2-type carbapenem-resistant *Klebsiella pneumoniae*. BMC Microbiol. 25, 676.

Kim, J.H., Jeong, Y., Lee, C.K., Kim, S.B., Yoon, Y.K., Sohn, J.W., Kim, M.J., 2020. Characteristics of *Klebsiella pneumoniae* isolates from stool samples of patients with liver abscess caused by hypervirulent *K. pneumoniae*. J. Kor. Med. Sci. 35, e18.

Kumar, S., Stecher, G., Li, M., Knyaz, C., Tamura, K., 2018. Mega X: molecular evolutionary genetics analysis across computing platforms. Mol. Biol. Evol. 35, 1547–1549.

Li, M., Guo, M., Chen, L., Zhu, C., Xiao, Y., Li, P., Guo, H., Chen, L., Zhang, W., Du, H., 2020. Isolation and characterization of novel lytic bacteriophages infecting epidemic carbapenem-resistant *Klebsiella pneumoniae* strains. Front. Microbiol. 11, 1554.

Li, P., Guo, G., Zheng, X., Xu, S., Zhou, Y., Qin, X., Hu, Z., Yu, Y., Tan, Z., Ma, J., Chen, L., Zhang, W., 2024a. Therapeutic efficacy of a K5-specific phage and depolymerase against *Klebsiella pneumoniae* in a mouse model of infection. Vet. Res. 55, 59.

Li, P., Zhou, Y., Guo, G., Qin, X., Hu, Z., Li, M., Tan, Z., Liu, Y., Han, X., Ma, J., Du, H., Zhang, W., 2024b. Efficacy of a new K3-specific bacteriophage for controlling *Klebsiella pneumoniae* in milk and its potential to disrupt biofilm formation. Food Control 163, 110519.

Liao, Y., Gong, J., Yuan, X., Wang, X., Huang, Y., Chen, X., 2024. Virulence factors and carbapenem-resistance mechanisms in hypervirulent *Klebsiella pneumoniae*. Infect. Drug Resist. 17, 1551–1559.

Lin, J.Y., Zhu, Z.C., Zhu, J., Chen, L., Du, H., 2024. Antibiotic heteroresistance in *Klebsiella pneumoniae*: definition, detection methods, mechanisms, and combination therapy. Microbiol. Res. 283, 127701.

Lin, M., Xiong, L., Li, W., Xiao, L., Zhang, W., Zhao, X., Zheng, Y., 2025. Isolation and identification of a newly discovered broad-spectrum Acinetobacter baumannii phage and therapeutic validation against pan-resistant Acinetobacter baumannii. Virol. Sin. 40 (4), 587–600.

Ma, Q., Zhu, Z., Liu, Y., Wang, J., Pan, Z., Yao, H., Ma, J., 2023. Keeping alert to the hypervirulent K1, K2, K3, K5, K54 and K57 strains of *Klebsiella pneumoniae* within dairy production process. Microb. Infect. 25, 105106.

McNair, K., Bailey, B.A., Edwards, R.A., 2012. PHACTS, a computational approach to classifying the lifestyle of phages. Bioinformatics 28, 614–618.

Mehta, T., Verma, S., Khangura, A.K., Mahapatra, N., Shrivastava, K., Gupta, S., 2025. Exploration of bacteriophage therapy as a viable alternative to combat antibiotic-resistant bacterial infections: a comprehensive *in vitro* and *in vivo* evaluation. Bioinformation 21, 2176–2180.

Mohammed, M.T., Zgair, A.K., 2025. Polymer matrix of biofilm in *Klebsiella pneumoniae* reduced by sub-MIC hydrogen peroxide enhances cefotaxime efficacy. Polim. Med. 55, 113–122.

Monegro, A.F., Muppidi, V., Regunath, H., 2025. Hospital-Acquired Infections (Archived). StatPearls. StatPearls Publishing, Treasure Island (FL).

Moraru, C., Varsani, A., Kropinski, A.M., 2020. VIRIDIC-A novel tool to calculate the intergenomic similarities of prokaryote-infecting viruses. Viruses 12, 1268.

Psonis, J.J., Michelen, Y., Banerjee, K., Fries, B.C., Sae-Tia, S., 2022. Cryptogenic liver abscess caused by a K1 Serotype *Klebsiella pneumoniae* isolate. J. Global Infect. Dis. 14, 117–119.

Russo, T.A., Marr, C.M., 2019. Hypervirulent *Klebsiella pneumoniae*. Clin. Microbiol. Rev. 32, e00001-19.

Senhaji-Kacha, A., Bernabéu-Gimeno, M., Domingo-Calap, P., Aguilera-Correa, J.J., Seoane-Blanco, M., Otaegi-Ugartemendia, S., van Raaij, M.J., Esteban, J., García-Quintanilla, M., 2024. Isolation and characterization of two novel bacteriophages

against carbapenem-resistant *Klebsiella pneumoniae*. Front. Cell. Infect. Microbiol. 14, 1421724.
Shi, L., Su, Y., Li, Z., Xiang, L., Liu, S., Li, X., Fu, L., Zhou, Y., 2026. Characterization of a phage vB_LZ 2044 deriving from K1-Type hypervirulent *Klebsiella pneumoniae* efficient against liver infection mice model. Probiotics Antimicrob. Proteins 18 (2), 1826–1836.
Sun, L., Xu, B., Tao, Y., Liang, Y., Chen, X., 2025. Exploring intervention strategies for microbial biofilms in the food industry based on a biomolecular mechanism perspective: recent advances and emerging trends. Foods 14, 4192.
Vuotto, C., Longo, F., Balice, M.P., Donelli, G., Varaldo, P.E., 2014. Antibiotic resistance related to biofilm Formation in *Klebsiella pneumoniae*. Pathogens 3, 743–758.
Wang, L., Shen, D., Wu, H., Ma, Y., 2017. Resistance of hypervirulent *Klebsiella pneumoniae* to both intracellular and extracellular killing of neutrophils. PLoS One 12, e0173638.
Zagaliotis, P., Michalik-Provasek, J., Gill, J.J., Walsh, T.J., 2022. Therapeutic bacteriophages for gram-negative bacterial infections in animals and humans. Pathog. Immun. 7, 1–45.
Zeng, J., Wan, X., Liu, T., Xiong, Y., Xiang, G., Peng, Y., Zhu, R., Zhou, Y., Liu, C., 2021. Chlorogenic acid ameliorates *Klebsiella pneumoniae*-induced pneumonia in immunosuppressed mice via inhibiting the activation of NLRP3 inflammasomes. Food Funct. 12, 9466–9475.